Fatigue Crack Propagation Analysis of Orthotropic Steel Bridge with Crack Tip Elastoplastic Consideration

Ying WANG[1], Zheng YAN[1], Zhen WANG[2]

(1 Jiangsu Key Laboratory of Engineering Mechanics, Southeast University, Nanjing, China, 211189)

(2 China Railway Major Bridge Reconnaissance and Design Institute Co. Ltd, Wuhan, China, 430056)

Corresponding author:

Ying WANG, Jiangsu Key Laboratory of Engineering Mechanics, Southeast University, Nanjing 211189, P.R. China.

Email: civil_wangying@seu.edu.cn

Abstract: Due to the complex structure of the orthogonal steel bridge deck and dense weld, fatigue cracks are prone to occur in the typical welding details. Welding residual stress will cause a plastic zone at the crack tip. In this paper, an elastoplastic constitutive model of *Chaboche* material was introduced, and the extended finite element method (XFEM) was used to study the influence of material elastoplasticity and crack tip plastic zone on the law of fatigue crack propagation. By judging the stress state of the residual stress field at the crack tip and selecting different crack propagation rate models to investigate the crack propagation law when plastic deformation was considered, the propagation path and propagation rate of fatigue crack of the orthotropic bridge deck were obtained. The results show that, whether the residual stress field is considered or not, the plastic deformation at the crack tip will not cause the obvious closure of the fatigue crack at the U-rib toe during the crack propagation process, but will significantly affect the crack propagation path. When material plasticity is considered, the propagation angle of fatigue crack at the U-rib toe basically remains unchanged along the short-axis direction of the initial crack, but increases along the long-axis direction, and the crack tip plastic zone inhibits the propagation of the crack tip on one side. Compared with linear elastic materials, the crack propagation law considering material plasticity is more consistent with the actual fatigue crack propagation law in bridge engineering. In terms of the propagation rate, if the residual stress field is not considered, the fatigue crack propagation rate at U-rib toe with plasticity considered is slightly higher than that without plasticity considered, because plastic deformation will affect the amplitude of energy release rate. When considering the welding residual stress field, the fatigue crack propagation rate at U-rib toe is increased due to the combined actions of plastic deformation and stress ratio *R*.

Keywords: Extended Finite Element; Fatigue Crack Propagation; Orthotropic Bridge Deck; Welding Residual Stress; Plastic Deformation;

Introduction

Due to its characteristics of light deadweight and high strength-to-weight ratio, orthotropic steel bridge deck (OSBD) have been widely used in large and medium span bridges[1-2]. Due to the complex structure and dense weld, fatigue cracks are easy to occur in typical welding details. With the increase of traffic flow and vehicle load year by year, coupled with the influence of welding residual stress in welding details, the cracks continue to propagate until the bridge deck crack failure. At present, finite element method, crack propagation software (NASGRO, AFGROW, ABAQUS, etc.) and energy release rate theory are mainly used for numerical simulation of fatigue crack and crack propagation of bridge deck [3-9]. In view of the influence of welding residual stress on the fatigue crack propagation of orthotropic bridge deck, *Wang* et al.[10] introduced the welding residual stress field into the segment model of steel bridge deck, and based on the extended finite element method (XFEM), studied the cracking mechanism and propagation law of typical fatigue crack of OSBD under the coupling effect of vehicle load and welding residual stress. *Zhou* [11] established the finite element model of fatigue crack at the butt weld of roof, longitudinal rib, transverse diaphragm and U-rib, and obtained the stress intensity factor of the crack front by combining the interaction integral and finite element method.

The results show that the type I stress intensity factor K_I is equivalent to the equivalent stress intensity factor K_{eff} in the fatigue crack propagation process of longitudinal rib butt weld, and the type I (open type) cracking mode is dominant in the process of fatigue crack propagation. K_I has been in the trend of increasing. Since stress intensity factor is the main parameter of crack propagation rate, fatigue crack rate increases gradually with crack propagation. The above researches rarely consider the plastic restraint effect or crack closure effect in the crack tip plastic region during crack propagation. In fact, when considering the welding residual stress at the weld, the stress in the weld zone of the orthotropic bridge deck may reach the yield strength of the material, indicating that the material has entered plasticity at this time. Even if the welding residual stress does not exceed the yield strength, the material near the crack will inevitably enter into plasticity with the fatigue crack propagation at the toe or root. *Qu* et al.[12] used discontinuous Galerkin XFEM to analyze the crack propagation hysteresis in bridge structure under overload condition, established a Q345Q slab model for bridge structural, and studied the influence of the plastic zone of the mode I crack on the crack propagation, but the research object is limited to structural steel, and the influence of the plastic zone of the typical fatigue crack on the crack propagation law of the whole bridge structure is not studied.

Therefore, for the whole structure of the bridge, this paper focuses on the change of fatigue crack propagation law caused by welding residual stress field and crack tip plastic zone. Considering that the U-rib welding toe at the joint of U-rib-diaphragm was significantly affected by welding residual stress, the fatigue crack propagation law of U-rib-toe in the whole bridge structure was mainly studied in this paper. To this end, the multi-scale finite element model of long-span bridge is firstly established, which includes the overall finite element model of the bridge with a characteristic scale of 10^2m, the tower with a characteristic scale of 10^0m, the deck system and cable model, and the fatigue crack model at the U-rib welding toe with a characteristic scale of 10^{-3}m. Then, the residual stress field was simulated based on commercial software ABAQUS. Finally, the XFEM is used to study the propagation law of fatigue crack at U-rib toe under the action of vehicle load alone and the residual stress field and vehicle load together when the material near the crack is plastic.

1 Fatigue crack propagation theory

1.1 Interaction integral calculation of residual stress intensity factor

Considering that the extended finite element module in ABAQUS finite element software cannot directly calculate the energy release rate corresponding to the beginning and end of each load cycle, the stress intensity factor at the beginning and end of each load cycle is calculated based on the interaction integral method, so as to further obtain the energy release rate. Interaction integral is a new calculation method developed on the basis of *J* integral, which not only inherits the advantages of simple and high precision of *J* integral calculation, but also solves the deficiency that *J* integral cannot directly obtain the crack tip stress intensity factor of composite crack. The basic assumption is that the cracked member bears two kinds of loads at the same time, namely the real load and the auxiliary load. The mechanical field at the crack tip is real (σ_{ij} , ε_{ij} , $u_{j,1}$). Under the action of the auxiliary load alone, the mechanical field at the crack tip is the auxiliary field $\left(\sigma_{ij}^{aux}, \varepsilon_{ij}^{aux}, u_{j,1}^{aux}\right)$. The auxiliary field of the crack tip is any possible displacement field and stress field satisfying the equilibrium condition, physical equation and geometric relation, while the real field of the crack tip is the actual displacement field and stress field of the crack tip to be studied. The two fields are superimposed to calculate the integral, and the *J* integral of the two fields acting alone is removed, leaving the interaction integral of the real field and the auxiliary field.

The location of the crack tip should be determined first when the interaction integral is used to solve the stress intensity factor. In the XFEM, the position of the crack surface is traced and defined by the level set function.The normal horizontal set function represents the vertical distance between the element node and the crack face.The extended finite element module in ABAQUS software can directly output the value of the node's normal level set function, but cannot directly output the coordinates of the crack surface. Instead, the coordinates of the crack tip in the process of crack propagation can only be calculated indirectly according to the node's normal level set function, and then the location of the crack surface can be determined.

For orthogonally anisotropic steel bridge deck, arbitrary hexahedral eight-node elements are adopted in this paper, as shown in Fig.1. The edges of the element are all straight lines. Normal level set function φ is 0 at the crack surface, the node above the crack surface normal level set function is positive, the node below the crack surface normal level set function is negative. Select the two nodes i and j on the edge of the element, then the intersection coordinates of the crack surface and the edge of the element can be obtained by linear interpolation:

$$\mathbf{P} = \mathbf{P}_i + \frac{\varphi_i}{\varphi_i - \varphi_j} \times (\mathbf{P}_j - \mathbf{P}_i) \tag{1}$$

Where, $\mathbf{P}$ is the intersection coordinates of crack surface and cell edge, $\mathbf{P}=(x,y,z)$, $\mathbf{P}_i$ and $\mathbf{P}_j$ are the spatial coordinates of node i and node j, φ_i and φ_j are the normal level set functions of node i and node j. When φ_i and φ_j are both positive or negative, the calculated point $\mathbf{P}$ is outside the cell edge, at this point, the intersection coordinates are invalid, and only if $\varphi_i \times \varphi_j < 0$, the calculated intersection point coordinates are the effective crack tip positions. According to Equation (2), it can be judged whether the coordinate of intersection point is on the edge of the element. When the calculated point P coordinates satisfy equation (2), the intersection point coordinates are effective.

$$\left|\mathbf{P} - \mathbf{P}_i\right| + \left|\mathbf{P} - \mathbf{P}_j\right| = \left|\mathbf{P}_i - \mathbf{P}_j\right| \tag{2}$$

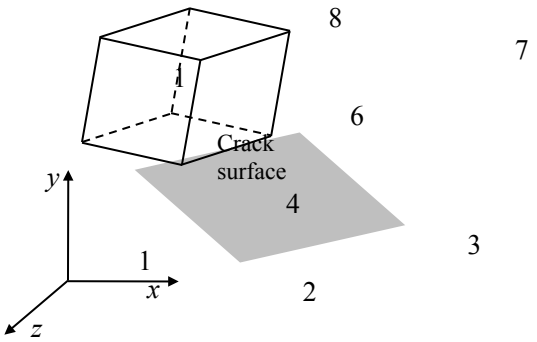

Fig. 1 Spatial location diagram of three-dimensional element and crack face

After the coordinate value of the crack tip is obtained, J integral is calculated by selecting the integral region of the crack tip. For the 3D model, the integral region of the J integral is shown in Fig. 2. In the inner boundary of volume V, the weight function q =1. The outer boundary of the volume domain, the weight function q=0. The formula of J integral [13] is:

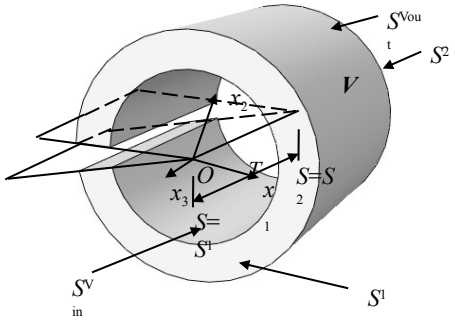

Fig. 2 three-dimensional J integral region[14]

$$J = \int_V \left(\sigma_{ij} u_{j,1} - W \delta_{1i} \right) \frac{\partial q}{\partial x_i} dV \tag{3}$$

Where δ_{ij} is the *Kronecker delta* function, and W is the strain energy density, as shown in Equation (4) :

$$W = \frac{1}{2} \sigma_{ij} \varepsilon_{ij} = \frac{1}{2} C_{ijkl} \varepsilon_{ij} \varepsilon_{kl} \tag{4}$$

Where C_{ijkl} is the stiffness matrix;

In fracture mechanics theory, the relation between J integral and stress intensity factor is shown in Equation (5):

$$J = \frac{1}{E'} (K_I^2 + K_{II}^2) + \frac{1+\mu}{E'} K_{III}^2 \tag{5}$$

Where E' is elastic modulus E in the plane stress state, and it is $E/(1-\mu^2)$ in the plane strain state, μ is Poisson's ratio.

Based on the J integral, interaction integral I introduces the mechanical field at the crack tip under the separate action of auxiliary load, namely the auxiliary field $\left(\sigma_{ij}^{aux}, \varepsilon_{ij}^{aux}, u_{j,1}^{aux} \right)$, so as to form a new J integral compound field J^{int} superposed by the real field and the auxiliary field at the crack tip, as shown in Equation (6) :

$$\begin{aligned} J^{int} &= \int_V \left[\left(\sigma_{ij} + \sigma_{ij}^{aus} \right) \left(u_{j,1} + u_{j,1}^{aus} \right) - \frac{1}{2} \left(\sigma_{jk} + \sigma_{jk}^{aus} \right) \left(\varepsilon_{jk} + \varepsilon_{jk}^{aus} \right) \delta_{1i} \right] q_{,i} dv \\ &= \int_v \left[\sigma_{ij} u_{j,1} - \frac{1}{2} \sigma_{jk} \varepsilon_{jk} \delta_{1i} \right] q_{,i} dv + \int_v \left[\sigma_{ij}^{aux} u_{j,1}^{aux} - \frac{1}{2} \sigma_{jk}^{aux} \varepsilon_{jk}^{aux} \delta_{1i} \right] q_{,i} dv \\ &\quad + \int_v \left[\left(\sigma_{ij} u_{j,1}^{aus} + \sigma_{ij}^{aus} u_{j,1} \right) - \frac{1}{2} \left(\sigma_{jk} \varepsilon_{jk}^{aus} + \sigma_{jk}^{aus} \varepsilon_{jk} \right) \delta_{1i} \right] q_{,i} dv \\ &= J + J^{aux} + I \end{aligned} \tag{6}$$

Where σ_{ij} , ε_{ij} , $u_{j,1}$ are the true fields, σ_{ij}^{aus} , ε_{ij}^{aus} , $u_{j,1}^{aus}$ are the auxiliary fields, J is the J integral of the action of the real field alone; J^{aus} is the J integral of the action of the auxiliary field alone, I is the part of the interaction between the real field and the auxiliary field, namely, the integral of the interaction.

The auxiliary field of the crack tip is obtained according to Westergaard stress function, and its displacement field is shown in Equation (7) :

$$
\begin{aligned}
u(r,\theta) &= \frac{1+\nu}{E}\sqrt{\frac{r}{2\pi}}\left\{K_{\mathrm{I}}\cos\frac{\theta}{2}\left[\kappa-1+2\sin^2\frac{\theta}{2}\right]+K_{\mathrm{II}}\sin\frac{\theta}{2}\left[\kappa+1+2\cos^2\frac{\theta}{2}\right]\right\}\\
v(r,\theta) &= \frac{1+\nu}{E}\sqrt{\frac{r}{2\pi}}\left\{K_{\mathrm{I}}\sin\frac{\theta}{2}\left[\kappa+1-2\cos^2\frac{\theta}{2}\right]+K_{\mathrm{II}}\cos\frac{\theta}{2}\left[\kappa-1-2\sin^2\frac{\theta}{2}\right]\right\}\\
w(r,\theta) &= \frac{2K_{\mathrm{III}}(1+\nu)}{E}\sqrt{\frac{r}{2\pi}}\sin\frac{\theta}{2}
\end{aligned}
\tag{7}
$$

Among them:

$$
\kappa=\begin{cases}3-4\nu & Plane\ strain\\ \dfrac{3-\nu}{1+\nu} & P\,lane\ stress\end{cases}
\tag{8}
$$

According to Formula (6), the interaction integral expression can be written:

$$
I=\int_v\left(\sigma_{ij}u^{aux}_{j,1}+\sigma^{aux}_{ij}u_{j,1}-\frac{1}{2}\left(\sigma_{jk}\varepsilon^{aux}_{jk}+\sigma^{aux}_{jk}\varepsilon_{jk}\right)\delta_{1i}\right)\frac{\partial q}{\partial x_i}dv
\tag{9}
$$

According to equation (5) of J integral and stress intensity factor, it can be seen that:

$$
J^{int}=\frac{1}{E'}(K_{\mathrm{I}}+K^{aux}_{\mathrm{I}})^2+\frac{1}{E'}(K_{\mathrm{II}}+K^{aux}_{\mathrm{II}})^2+\frac{1+\mu}{E'}(K_{\mathrm{III}}+K^{aux}_{\mathrm{III}})^2=J+J^{aux}+I
\tag{10}
$$

The relationship between interaction integral I and stress intensity factor is shown in Equation (11) :

$$
I=\frac{2}{E'}(K_{\mathrm{I}}K^{aux}_{\mathrm{I}}+K_{\mathrm{II}}K^{aux}_{\mathrm{II}})+\frac{2(1+\mu)}{E}K_{\mathrm{III}}K^{aux}_{\mathrm{III}}
\tag{11}
$$

Stress intensity factor of the real displacement field can be got by controlling K^{aux}_{I} ,K^{aux}_{II} , K^{aux}_{III} in virtual displacement field. $I_{(1)}$ can be got when $K^{aux}_{\mathrm{I}}=1$, $K^{aux}_{\mathrm{II}}=K^{aux}_{\mathrm{III}}=0$; $I_{(2)}$ can be got when $K^{aux}_{\mathrm{II}}=1, K^{aux}_{\mathrm{I}}=K^{aux}_{\mathrm{III}}=0$ $I_{(3)}$ can be got when $K^{aux}_{\mathrm{III}}=1, K^{aux}_{\mathrm{I}}=K^{aux}_{\mathrm{II}}=0,$ so the stress intensity factor of the real displacement field is shown in Equation (12) :

$$
K_{\mathrm{I}}=\frac{E'}{2}I_{(1)}\ ,\quad K_{\mathrm{II}}=\frac{E'}{2}I_{(2)}\quad K_{\mathrm{III}}=\frac{E}{2(1+\mu)}I_{(3)}
\tag{12}
$$

The discrete integral formula for calculating the J integral in the integral volume V element by finite element method is shown in Equation (13) :

$$
J=\sum_{e}^{elems}\sum_{p}^{gps}\left\{\begin{aligned}&\left[\left(\sigma_{xx}\frac{\partial u}{\partial x}+\tau_{xy}\frac{\partial v}{\partial x}+\tau_{xz}\frac{\partial v}{\partial x}-W\right)\frac{\partial q}{\partial x}+\left[\tau_{xy}\frac{\partial u}{\partial x}+\sigma_{yy}\frac{\partial v}{\partial x}+\tau_{yz}\frac{\partial w}{\partial x}\right]\frac{\partial q}{\partial y}\right.\\&\left.+\left[\tau_{zx}\frac{\partial u}{\partial x}+\tau_{yz}\frac{\partial v}{\partial x}+\sigma_{zz}\frac{\partial w}{\partial x}\right]\frac{\partial q}{\partial z}\right\}\det J_e
\end{aligned}
\tag{13}
$$

Where, V is the integral volume region, and elems is the number of all elements in the integral volume V. P is integral point, gps is the number of unit integral points. For a hexahedral eight-nodal element, the integral form is

2×2×2 Gaussian integral, and the coordinate of the integral point is $\pm 1/\sqrt{3}$. $detJ_e$ is the determinant of the Jacobian matrix.

According to formula (13), the corresponding J integral is solved by combining the real displacement field, virtual displacement field and the sum of real and virtual displacement fields. The interaction integral I and the corresponding stress intensity factor are obtained according to Formula (12). The specific calculation flow chart is shown in Fig. 3. First, the element number, node number, node coordinates, normal level set function and node displacement in the integral volume V region of the crack tip are extracted from the results file of extended finite element analysis. The coordinates of the intersection point between the crack surface and the edge of the element are obtained by linear interpolation, and the crack tip position and the crack surface angle are determined. In order to get the exact value of the superposition of virtual displacement and real displacement, the coordinates of the nodes and their displacements were converted into coordinates, in the converted coordinate system, x axis was parallel to the crack surface and perpendicular to the crack front, y axis was perpendicular to the crack surface, and z axis was parallel to the crack surface and the crack front. The virtual displacement of the node was determined according to the displacement field of the crack tip obtained by Westergaard stress function, the virtual displacement field $U2$ had three cases, when $K_{\mathrm{I}}^{aux}=1, K_{\mathrm{II}}^{aux}=K_{\mathrm{III}}^{aux}=0$, the interaction integral I_1 was obtained; when $K_{\mathrm{II}}^{aux}=1, K_{\mathrm{I}}^{aux}=K_{\mathrm{III}}^{aux}=0$, the interaction integral I_2 is obtained; when $K_{\mathrm{III}}^{aux}=1, K_{\mathrm{I}}^{aux}=K_{\mathrm{II}}^{aux}=0,$ the interaction integral I_3 is obtained. The J integral values of real displacement, virtual displacement and total displacement of the node J_1, J_2 and J_3 are obtained by integrating the 8 Gauss integral points of all elements in the integral domain respectively, then the interaction integral $I=J_3-J_2-J_1$. By using different virtual displacement fields $U2$, the interaction integrals I_1, I_2 and I_3 of the three crack types can be obtained, and the stress intensity factors K_{I}, K_{II} and K_{III} of the real displacement fields can be obtained from formula (12).

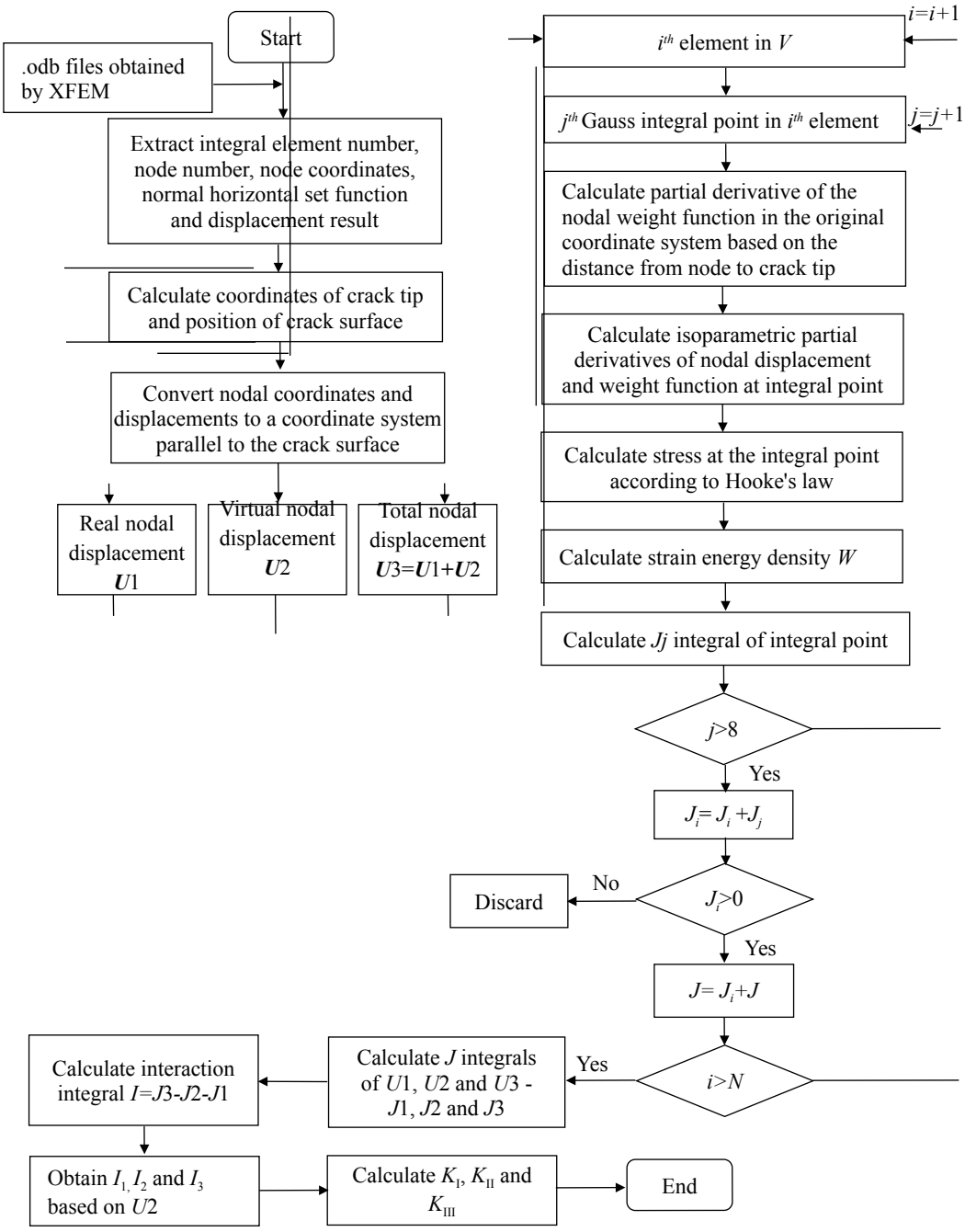

Fig. 3 Implementation process of interaction integral

1.2 Fatigue crack propagation analysis theory

In the ABAQUS finite element software, whether the fatigue crack starts is judged by the increase of energy release rate ΔG and the maximum value of energy release rate $G_{\max}$. When the energy release rate increment ΔG content type (14), and in the process of loading cycle, the maximum energy release rate of crack tip G_{max} exceeds the fatigue crack propagation threshold of steel G_{th}, the fatigue crack begins to propagate.

$$f = \frac{N}{c_1 \Delta G^{c_2}} \quad 1 \tag{14}$$

Where, c_1 and c_2 are material constants, and N is the number of cycles. When the above two crack propagation conditions are met, and the maximum energy release rate at the crack tip G_{max} is less than the upper limit G_{pl}, G_{pl} is close to the steel fracture toughness G_C, then the fatigue crack can propagate under the current cyclic load, and the

propagation law can be simulated by the fatigue crack propagation rate model.

Under the influence of welding residual stress, the fatigue crack propagation law can be obtained by *Walker*[15] formula, whose expression is:

$$\frac{da}{dN} = C\left[\frac{\Delta K}{(1-R)^{\gamma}}\right]^{m} \tag{15}$$

$$R = \frac{K_{\min}+K_r}{K_{\max}+K_r} \tag{16}$$

Where N is the number of cycles; a is the length of the crack; R is the stress ratio, K_{max} is the maximum stress intensity factor; K_{min} is the minimum stress intensity factor; K_r is the stress intensity factor under the influence of welding residual stress, C, n and m are material constants, which can be obtained from test or specification. The C and m selected in this paper refer to the Japanese JSSC specification [16], C=2*10^{-12}, m=2.75. In the fatigue crack propagation analysis of bridge steel, n*m is generally assumed to be 1[17].

The influence of stress ratio R on fatigue crack life is reflected in the *Walker* formula, but the influence of crack tip plasticity on fatigue crack propagation is not considered. In 1971, *Elber*[18] found through tests that the plastic deformation of crack tip would lead to the closure of crack surface, which hindered the action of external load on crack surface. The crack would continue to expand only after the crack face was fully opened. Aiming at the crack closure phenomenon, *Elber* proposed to use the stress intensity factor K_{op} corresponding to the crack opening stress to reflect the crack closure effect, taking the effective stress intensity factor ΔK_{eff} as the parameter of the fatigue crack propagation model, and proposed a fatigue crack propagation model considering the plasticity of the crack tip:

$$\frac{da}{dN} = C\left(\Delta K_{eff}\right)^{m}$$
$$\Delta K_{eff} = K_{\max} - K_{op} \tag{17}$$

The material constants C and m in the formula can take the corresponding values of *Paris* formula and *Walker* formula.

There are many methods for the solution of crack opening stress intensity factor K_{op} and opening stress σ_{op}, and three methods are commonly used in finite element analysis:

(1) Nodal displacement method [19] determines the opening stress by monitoring the displacement state of the first or second nodal point of the crack tip. In the loading stage, when the monitored nodal displacement becomes positive, the corresponding nodal stress is the opening stress ; (2) *Wu* and *Ellyin* [20] defined crack opening stress as the far-field stress at the crack tip node perpendicular to the crack plane that changes from compressive stress to tensile stress. (3) *Matos* [21] believes that the residual stress intensity factor generated in the plastic zone of crack tip is the stress intensity factor that needs to be overcome by crack opening stress. Therefore, the relationship between the residual stress intensity factor and crack opening stress intensity factor is shown in Equation (18):

$$K_{res} + K_{op} - K_{\min} = 0 \tag{18}$$

Where, K_{res} is the residual stress intensity factor, which can be solved by the interaction integration method.

When considering the welding residual stress field of components, especially the welding residual compressive stress at the crack tip, the fatigue crack propagation life can be analyzed based on the *Elber* crack

closure theory, Because *Elber*'s theory that the plastic deformation of the crack tip generates the residual compressive stress and the crack closure is essentially the same as the external compressive residual stress field causes the crack closure[22], the subtle difference is that the closure of the crack in the welding residual stress field is the result of the combined effect of the welding residual compressive stress and the crack tip plastic zone. At this time, the crack opening stress is the sum of the external welding residual compressive stress field and the residual compressive stress generated by the plastic zone at the crack tip.

In the finite element software ABAQUS, the energy release rate is taken as the parameter to analysis the fatigue crack propagation. In the fatigue crack propagation rate model of equations (17) and (18), the increment of stress intensity factor is replaced by the increment of energy release rate. The corresponding material constants C and m need to be transformed accordingly, the transformation relationship is shown in Equation (19):

$$C' = C\left(E'\right)^{m'}$$
$$m' = \frac{m}{2} \tag{19}$$

Where C' and m' are material constants when the energy release rate is taken as the parameter of the fatigue crack propagation model.

In this paper, after the stress intensity factor of the crack tip is obtained based on the interaction integration method, the residual stress state (tensile stress or compressive stress) of the crack tip is judged according to the positive and negative values of the stress intensity factor, then, different models of crack propagation rate are selected to calculate the number of load cycles, where the number of load cycles is N in *Paris* formula and described by the number of load cycles in ABAQUS. If the welding residual stress field at the crack tip is the tensile stress state, the load cycle N is calculated based on *Walker* formula. If the welding residual stress field at the crack tip is the compressive stress state or the residual compressive stress caused by plastic deformation, then the crack closure effect is considered and the number of load cycles N is calculated according to *Elber* formula. In this paper, the constitutive model of elastoplastic materials is *Chaboche* model, and its parameters are referenced [23], as shown in Table 1.

Table 1 parameters of *Chaboche* model

Q_∞/MPa	b	C_1/MPa	γ_1	C_2/MPa	γ_2	C_3/MPa	γ_3	C_4/MPa	γ_4
21	1.2	7993	175	6773	116	2854	34	1450	29

2 Description of finite element model

2.1 Finite element model to simulate welding process

A detailed solid element model of the joint of the U-rib-diaphragm containing the weld is established, as shown in Fig. 4. In the thermal analysis, the heat source uses a double ellipsoid heat source, and the parameters are shown in Table 2. The room temperature was set at 20°C, and the welding heating process was divided into 155 steps. A sub-step was set for every 0.2s, and the total heating time was 31s. The cooling process of the welding process was completed at 2100s. In the structural analysis, the displacement in the x direction is constrained by the U-rib along the positive direction of the x axis, the cross section of the diaphragm along the positive direction of the z axis is constrained by the symmetry, and the cross sections of the U-rib and the diaphragm along the negative direction of the y axis are constrained by the y-direction displacement.

Table 2 Parameters of double ellipsoid heat source function

Parameter	U-rib - roof joint	U-rib - diaphragm joint
Length of the front axle a_1/mm	3	6
Length of the front rear a_2/mm	5	14
b/mm	10	8
c/mm	18	5
Welding speed /mm·s^{-1}	10	10
Welding voltage U/v	350	250
Welding current I/A	35	25

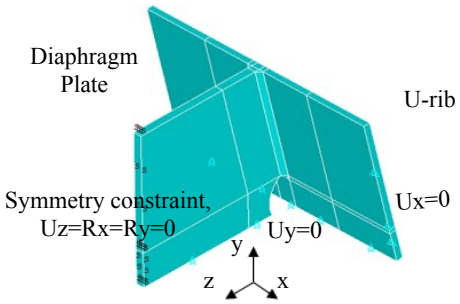

Fig. 4 Welding analysis model of the joint of U-rib and diaphragm plate

According to literature [24] and combined with literature [25], the thermal physical and thermodynamic parameters of steel used in welding analysis were appropriately modified to obtain the thermodynamic analysis parameters of Q345 steel used in this model, as shown in Fig. 5.

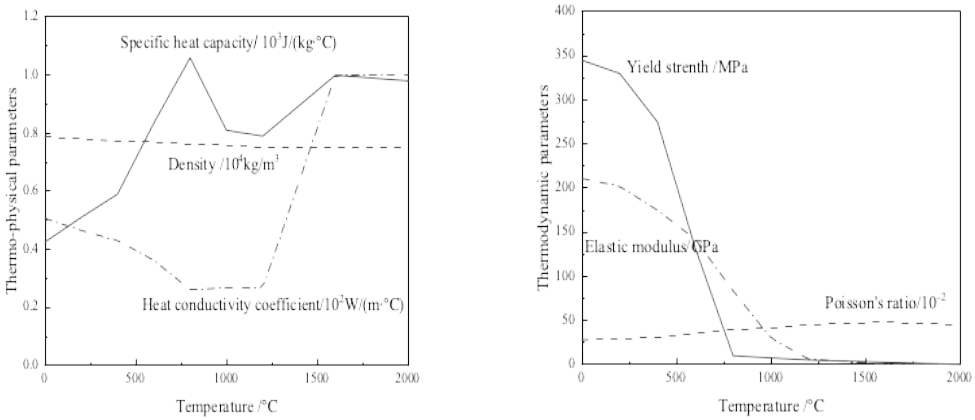

(a) Thermophysical parameters of Q345 steel (b) Thermodynamic parameters of Q345 steel

Fig. 5 Thermodynamic analysis parameters of Q345 steel

2.2 Multi-scale finite element model and loading condition of bridge

In order to study the stress characteristics and crack propagation rule of U-rib-diaphragm under vehicle load, a multi-scale finite element model of bridge was established. Taking the cable-stayed bridge of Runyang Yangtze River Highway Bridge in north Branch as an example, in the commercial finite element software ABAQUS, the integral finite element model of the bridge with a characteristic scale of 10^2m was first established, as shown in Fig. 6(a). The model includes a bridge tower, a cable and an OSBD. The concrete counterweight of steel box

girder at the end of the bridge is simulated by mass unit. Three translational and three rotational degrees of freedom are constrained at the end of the bridge and at the bottom of the bridge. The bridge tower is simulated by beam element B31, and the cable is simulated by rod element T3D2. In order to simplify the model and improve the calculation efficiency, according to the stiffness equivalence principle of composite mechanics, the orthogonal anisotropic bridge deck containing the U-rib is equivalent to the physically equivalent orthogonal anisotropic bridge deck without the U-rib [26]. The bridge deck is simulated by shell element S4, as shown in Fig. 6(b). In order to accurately obtain the fatigue stress characteristics of each structural detail of the steel box girder under cyclic vehicle load, considering that the middle part of the span is the part with large vertical displacement of the structure, the fine modeling was carried out for the steel bridge deck with a length of 40m in the middle span. Fig. 6(c) shows a meso-scale mesh refined model with the characteristic of 10^0m, including the shell element model of roof, floor, oblique web, anchorage zone, U-rib and diaphragm. Submodel technology is used to connect the boundary between the full-bridge model and the refined orthogonal anisotropic bridge deck model. The dislocations of the cut boundary nodes of the full-bridge model are linearly interpolated to the boundary nodes of the local model, and the dislocations of the nodes are coupled. The components of the refined model are simulated by shell element S4 or S3. The shell element cannot simulate the crack propagation behavior. In order to study the fatigue crack propagation along the direction of plate thickness, a solid model was established at the key parts of the bridge bearing the stress, including the joint of the U-rib and the crack, and C3D8 element was used to simulate it, as shown in Fig. 6(d). The established solid model is embedded into the corresponding position of the refined model of the orthotropic bridge deck in Fig. 6(c) to replace the original shell element model. The shell-solid element coupling connection is adopted between the embedded solid element model and the surrounding refined shell element. The length of U-rib is 300mm, the height is 200mm, and the width of transverse diaphragm is 150mm. In order to study the crack propagation behavior at the connection part of the U-rib-diaphragm, a semi-elliptical initial crack was established at the toe of the U-rib with a long axis of 10mm and a short axis of 2mm, and the characteristic scale of the crack was 10^{-3}m, as shown in Fig. 6(e).

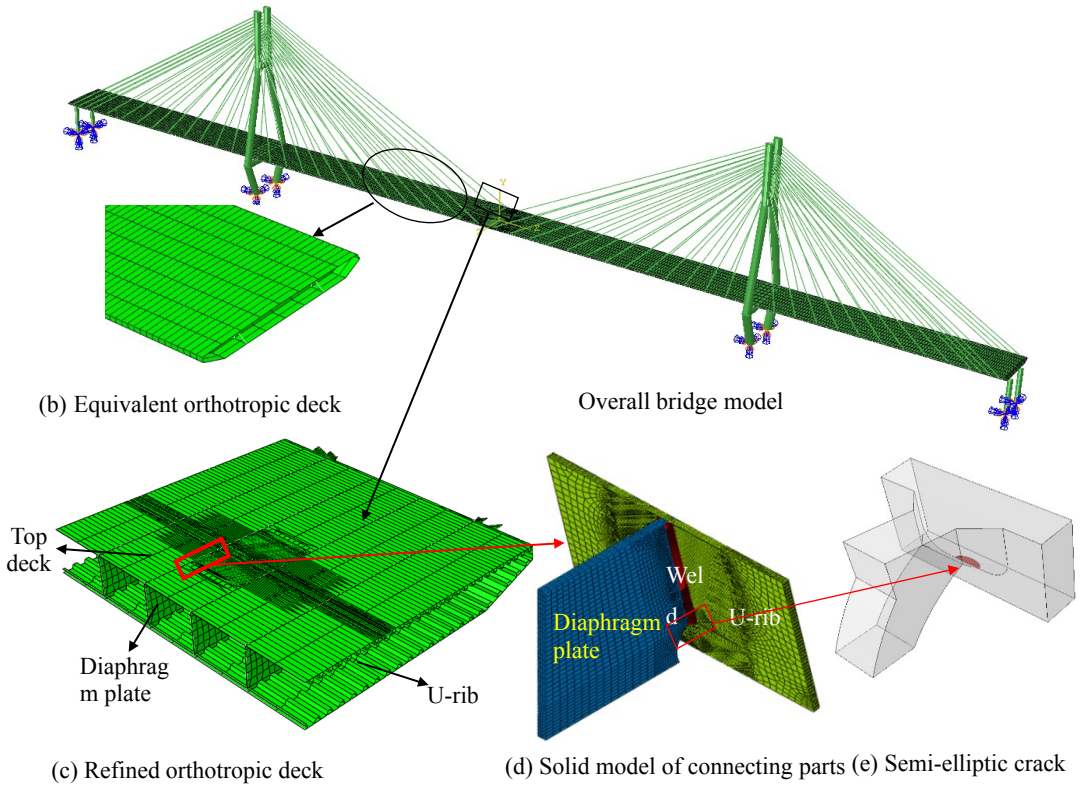

Fig 6. Runyang multi-scale finite element model of cable-stayed bridge

The vehicle load model selected in this paper refers to fatigue load model III[27] in《Highway Steel Structure Bridge Design Specification JTG D64-2015》, and its loading mode is shown in Fig. 7. The model consists of four standard axes. The distance between the longitudinal and longitudinal axes is 6m and the distance between them is large. For a node on the bridge face plate, when the wheel pressure of the two axes of the current plane acts near the node, the latter two axes are still far away from the point, which has no significant influence on the fatigue stress of this part. Therefore, this paper only takes the two-wheel pressures with a longitudinal wheelbase of 1.2m as the fatigue load applied to the multi-scale model of the bridge. The area of each wheel load acting surface is 0.2m×0.6m, and the total weight of vehicle load is 240KN. The loading location is shown in Fig. 8. At this position, the initial crack of the vehicle load wheel pressure A center along the transverse bridge is 0.1m away from the U-rib welding toe, and the initial crack along the longitudinal bridge is 0.75m away from the U-rib. The joint of the U-rib-diaphragm is between the front axle and the rear axle of the vehicle load.

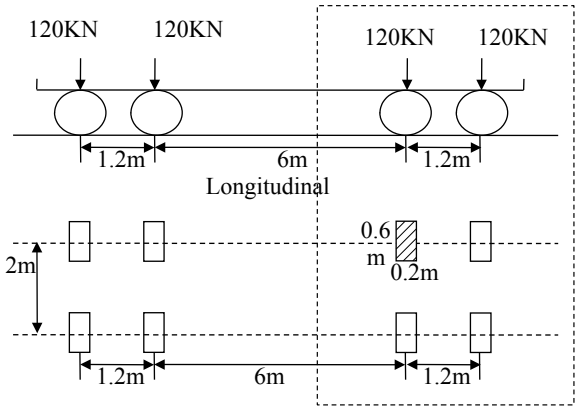

Fig. 7 Fatigue Load Model III [27]

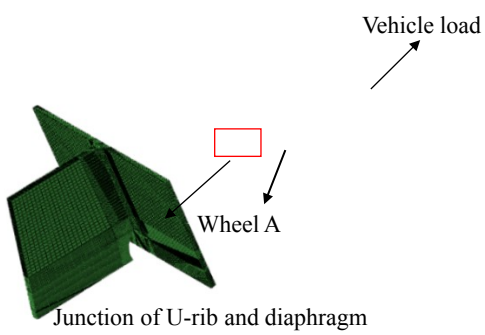

Fig. 8 The loading position of vehicle with fatigue crack at U-rib welding toe

3 Welding residual stress analysis

The welding residual stress field can be obtained through thermal-structural sequence coupling, as shown in Fig. 9. It can be seen that the equivalent stress of the whole weld area reaches the yield stress of steel. The residual stress at the beginning and end of the welding seam is small, the middle area of the welding seam is in the state of residual tensile stress, the stress distribution is uniform and has reached the steel yield stress. The distribution of residual stress on some typical paths of the U-rib-diaphragm connection is studied, the corresponding path diagram is shown in Fig.10. Path 1 is parallel to the U-rib toe and starts at the center of the U-rib toe, path 2 is perpendicular to the U-rib toe and starts at the center of the U-rib toe, path 3 is the cross-baffle toe, starting at the upper end of the cross-baffle toe, path 4 starts at the lower end of the cross-baffle toe and ends at the toe of the cross-baffle toe.

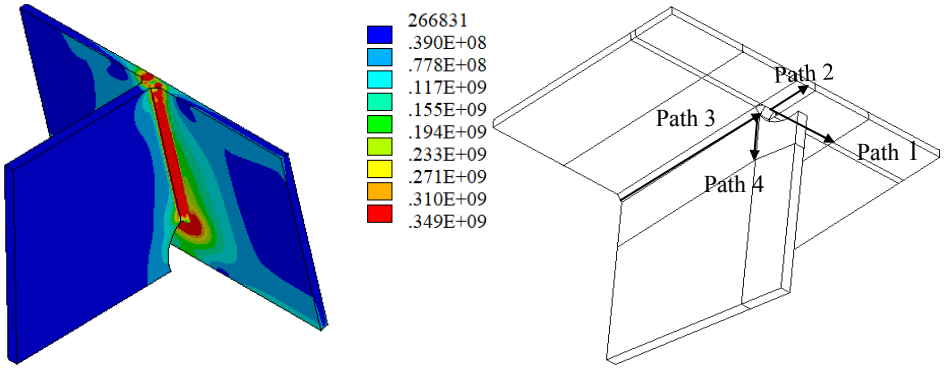

Fig. 9 Von Mises stress (unit: Pa) at the connections of U-rib-diaphragms

Fig. 10 Path diagram of the connections of U-rib-diaphragms

Fig. 11 shows the distribution curves of residual stress over four typical paths. Fig. 11(a) shows the transverse residual stress of path 1, and Fig. 11(b) shows the transverse residual stress of path 2. It can be seen that the transverse residual stress of the U-rib welding toe on path 1 and path 2 is relatively large at the U-rib welding toe, while the stress on the U-rib far from the U-rib gradually decreases, while the U-rib far from the center of the toe on path 1 is the residual compressive stress. Fig. 11(c) shows the distribution of transverse and longitudinal residual stresses in path 3. It can be seen that the transverse and longitudinal residual stresses at the toe of the diaphragm are the stable area of residual stress in the middle area of the toe, while the transverse and longitudinal residual stresses are almost all tensile stresses, and only the residual compressive stresses occur in the small area at the end of the toe of the diaphragm. By figure 11 (d) path 4 transverse and longitudinal residual stress as you can see, perpendicular to the horizontal clapboard on the path of the weld toe 4, diaphragm plate weld toe end of lateral and longitudinal residual stress to a minimum, with the increase of distance from the weld toe, the residual stress increased, then tends to a stable value, path on the 4 small, transverse and longitudinal tensile stress peak at about 100 MPa and 25 MPa, respectively. Fig. 11(e) and Fig. 11(f) show the residual stress at the toe of transverse diaphragm and the toe of U-rib, which were simulated in literature [25] and [10], respectively. This paper can be found by U-rib-diaphragm plate welding of longitudinal and transverse residual stress distribution rule and literature [10] and [25] gives the law of basic consistent, therefore, the residual stress of the simulation results can be thought of as accurate, for subsequent analysis U-rib-diaphragm connection costal toe regularity of fatigue

crack in the residual stress field provide the initial stress field.

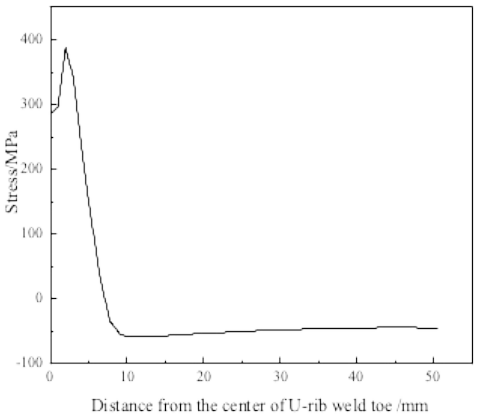

(a) Path 1 transverse residual stresses

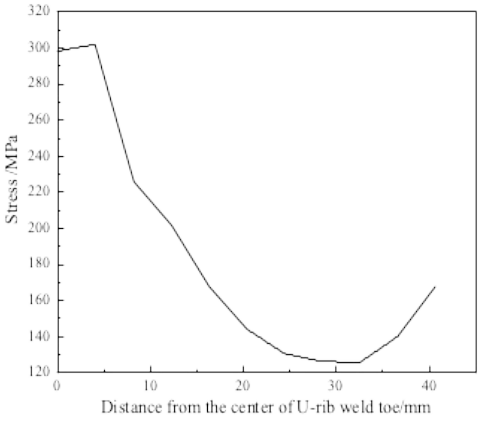

(b) Path 2 transverse residual stresses

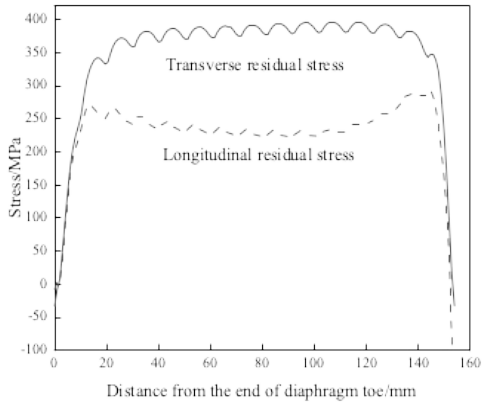

(c) Path 3 transverse and longitudinal residual stresses

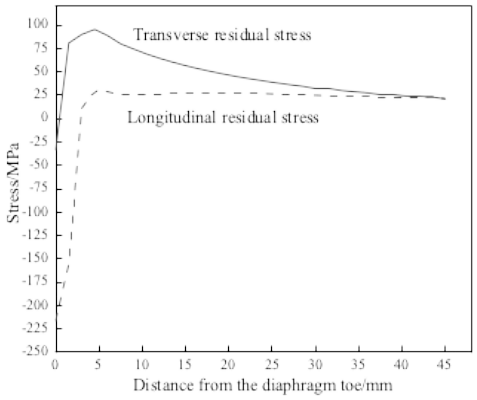

(d) Path 4 transverse and longitudinal residual stresses

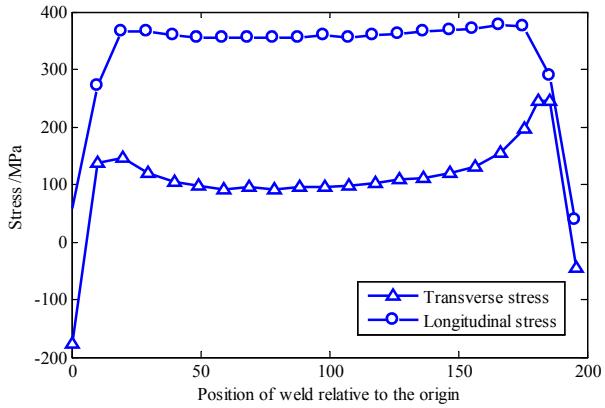

(e) Transverse and longitudinal welding residual stress of diaphragm toe [25]

(f) U-rib welding residual stress[10]

Fig. 11 Distribution curve of residual stress at the junction of U-rib-diaphragm

4 Analysis of fatigue crack propagation at U-rib toe

4.1 Fatigue crack propagation path

Firstly, without considering the influence of residual stress field of welding, cyclic vehicle load as shown in Fig. 9 is applied to the multi-scale finite element model of the bridge containing the initial crack, and the elastic-

plastic constitutive relation of the material is embedded, then, the fatigue crack propagation path at the U-rib toe was obtained by using the XFEM, as shown in Fig.12. It can be seen that when the plastic deformation of the material is considered but the influence of the residual stress field is not taken into account, the surface crack morphology caused by the plastic deformation is asymmetric to the center line of the diaphragm, and the crack front propagation rate on the right side is higher than that on the left side. In the long axis direction of the initial crack, the crack surface after expansion presents an angle of about 17° with the initial crack surface. In the short-axis direction of the initial crack, the crack extends along the depth of the U-rib to the roof with a small deflection angle, and the crack depth reaches 6mm after 3.5 million cycles. Before the load cycle of 2 million times, the fatigue crack at the U-rib welding toe mainly expanded along the long axis direction of the initial crack. When the loading cycle is between 2 million and 3.5 million times, the crack propagates mainly along the short axis of the initial crack.

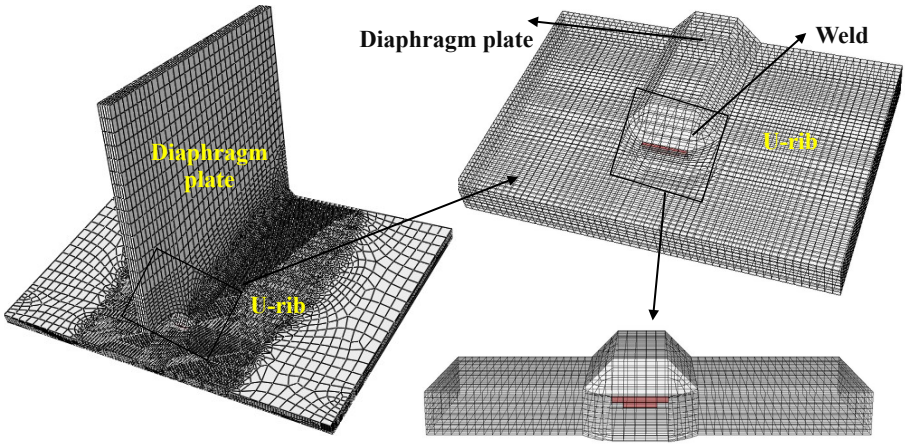

(a) Initial crack surface

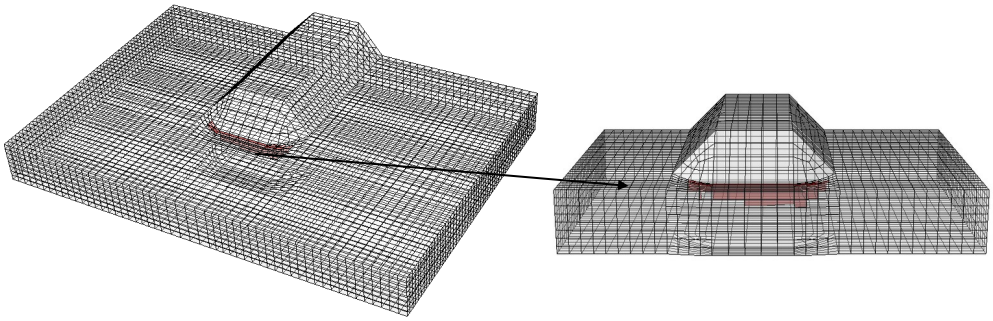

(b) 600,000 cycles

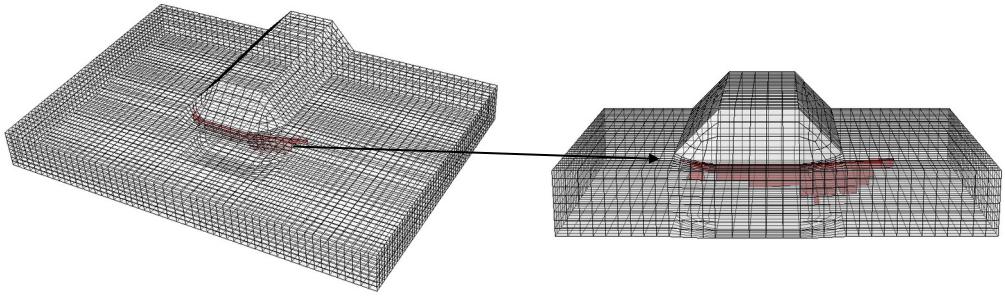

(c) 2 million cycles

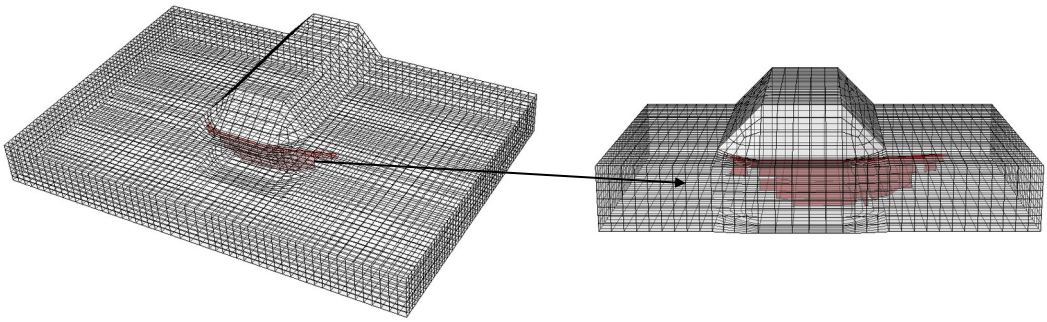

(d) 3.5 million cycles

Fig. 12 Fatigue crack propagation path at U-rib welding toe without considering residual stress field (plastic material)

Similarly, when plastic deformation of materials and the influence of welding residual stress field are considered, cyclic vehicle loads are applied to the multi-scale finite element model of the bridge to obtain the propagation path of fatigue crack at the U-rib welding toe, as shown in Fig. 13. It can be seen that the propagation rate of the fatigue crack leading edge on the left side is higher than that on the right side before the load cycle of 30,000 times, with the center line of the diaphragm as the boundary. After 30,000 cycles, the leading edge position of the left crack basically remained unchanged, and the crack propagation rate on the right side was higher than that on the left side. At the end of the load cycle, the crack on the right side of the diaphragm was extended longer with the Central Line of the diaphragm as the boundary. As can be seen from Fig. 13, the fatigue crack propagation law of U-rib toe in the short-axis direction is similar in the two cases. Taking the initial crack surface as the reference, the cracks all spread in the direction of the roof with micro-deflection angle, and the crack length along the short-axis direction was 6mm at the end of the cycle. However, when residual stress is taken into account, the crack propagation angle in the long axis direction is large. By extracting the coordinate information of the crack, the included angle between the crack propagation path along the long axis of the initial crack and the initial crack is 67.5°.

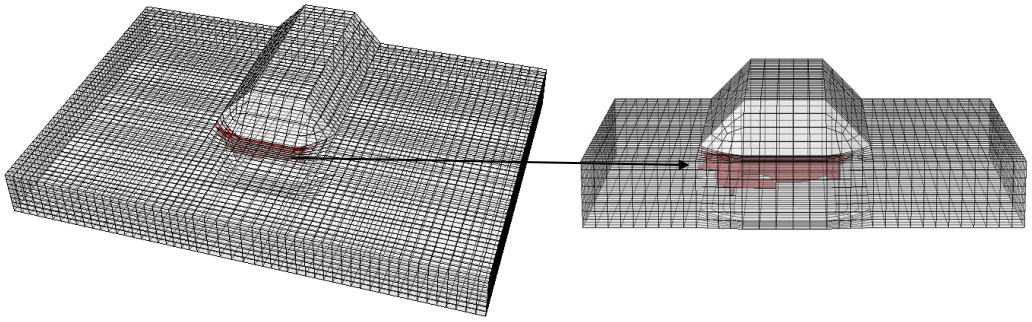

(a) 30,000 cycles

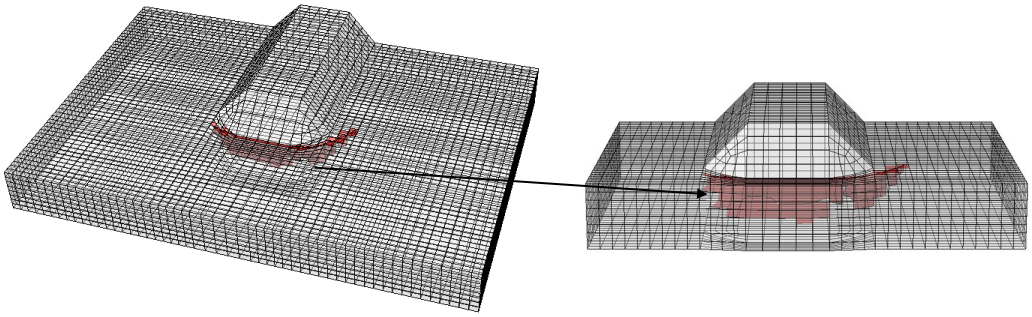

(b) 200,000 cycles

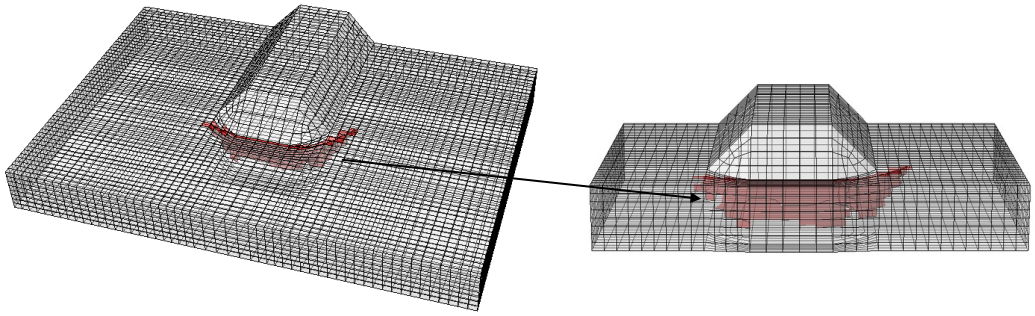

(c) 250,000 cycles

Fig. 13 Fatigue crack propagation path at U-rib welding toe considering residual stress field (plastic material)

The fatigue crack propagation paths of U-rib toe were compared under the following four conditions: considering residual stress and material plasticity, considering residual stress and material elasticity, not considering residual stress and material plasticity, not considering residual stress and material elasticity. The fatigue crack propagation steps at U-rib toe under four conditions were set as 90 steps. The propagation step represents the number of crack propagation. In the extended finite element analysis, ABAQUS software can obtain the value of stress intensity factor corresponding to all elements at the leading edge of the crack each time the load is applied, and then the life of each element N can be obtained according to Paris formula. Since there is more than one element at the leading edge of the crack, the program will set cracking of the element with the minimum life N and no cracking of the other elements, that is, only one element at the leading edge of the crack will generally propagate at each fatigue crack propagation step. The coordinates of the leading edge of the crack were extracted. Fig. 15 shows the fatigue crack propagation path at U-rib toe under different conditions. Fig. 14(a) shows the difference in fatigue crack propagation paths caused by plasticity and elasticity when residual stress fields are considered. It can be seen that, considering material to plastic deformation, U-rib on the left side of the crack tip due to large plastic zone inhibits the crack extension, with transverse diaphragm axis is bounded, fatigue crack in the diaphragm plate on the right side of the crack tip length increment is bigger, and the initial crack extension along the long axis angle also increases, after considering plastic deformation crack angle by 59 ° increase to 67.5 °. Fig.14(b) shows the difference in fatigue crack propagation paths caused by plasticity and elasticity of materials without considering the residual stress field. It can be seen that when material plasticity is considered, the crack increment at the left crack tip of U-rib is slightly smaller than that when material elasticity is considered, indicating that when plasticity is considered, the plastic zone of the left crack tip of U-rib also restricts crack propagation. However, due to small plastic deformation, the inhibition effect is obvious when residual stress field is not considered. In terms of the crack propagation angle, the crack angle increases from 0° to 17° when considering the plasticity of the material. Under the same crack propagation step, the U-rib fatigue crack increases more in the crack length along the long axis when considering the plastic deformation.

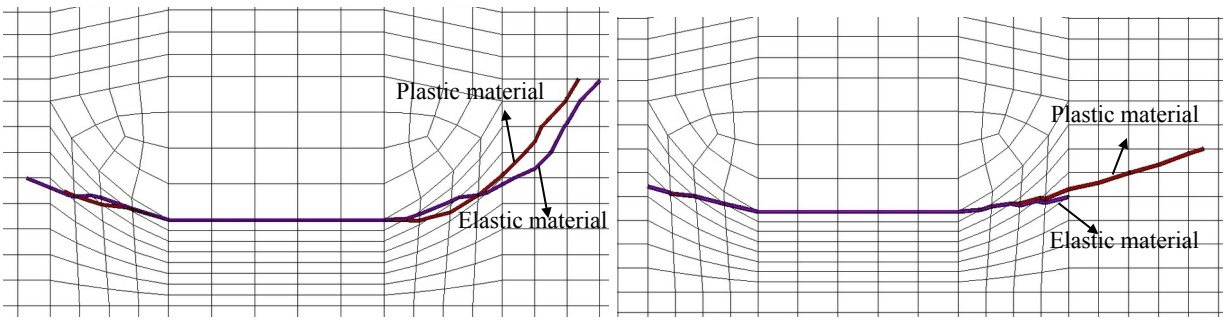

(a) Consider the residual stress field (b) Without considering residual stress field

Fig. 14 Fatigue crack propagation path at U-rib toe under different conditions

4.2 Analysis of residual stress intensity factor

Based on the elastic-plastic analysis of fatigue crack in U-rib toe, the crack opening stress intensity factor K_{op}, namely, type I crack stress intensity factor K_{I}, was obtained without considering the residual stress field. When the welding residual stress field is not considered, the external load will also cause the crack tip to produce plastic deformation and then the residual compressive stress. According to the node displacement field in the integral domain of the interaction integral, the residual stress intensity factor K_{res} is calculated as a negative value. However, according to formula (18), the sum of crack opening stress intensity factor K_{op} and residual stress intensity factor K_{res} is zero, and the positive crack opening stress intensity factor is finally obtained, as shown in Fig. 15. When there is no residual stress field, the U-rib fatigue crack is at the initial stage of crack propagation, and the stress at the connection part of the U-rib-diaphragm does not reach the yield stress before 200,000 load cycles, and there is no plastic deformation at the crack tip. Therefore, the crack opening stress intensity factor in Fig. 16 is always zero before 200,000 cycles. With the crack propagation, the plastic strain only appears in the very small area of the crack tip, and the plastic region is far less than the crack length, and the ultimate crack opening stress intensity factor is very small, the maximum value is only $0.4\mathrm{Mp}\cdot\mathrm{m}^{0.5}$, and the energy release rate converted into $0.8\mathrm{N}\cdot\mathrm{m}^{-1}$, which is far less than the amplitude of the energy release rate generated by the cyclic vehicle load, this indicates that the crack opening stress caused by plastic deformation has little influence on the fatigue crack propagation of U-rib and can be ignored when there is no residual stress field.

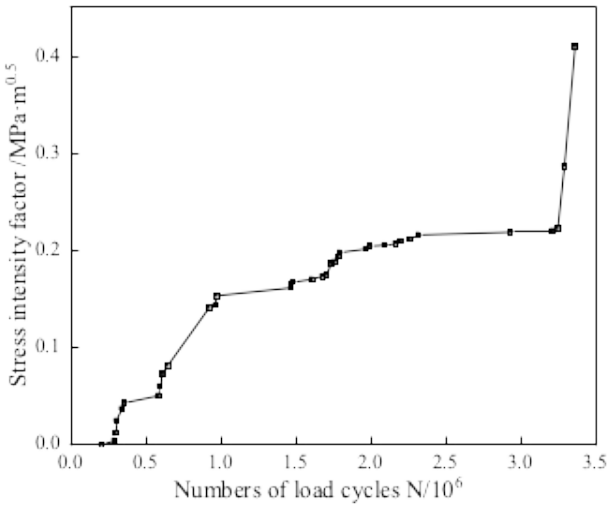

Fig. 15 Crack opening stress intensity factor K_I at U-rib weld toe without residual stress field

When the residual stress field is introduced, the crack tip stress field of the fatigue crack at the U-rib toe reaches the yield stress of the material before the crack propagation. In the process of crack propagation, the crack propagation step with a large plastic zone is selected to obtain the equivalent plastic strain in the crack tip region of the U-rib, as shown in Fig. 16. In order to observe the plastic zone range of the crack tip more intuitively, the strain cloud map given in Fig. 16 does not show the plastic strain at the crack surface. If the plastic strain at the crack surface is shown, the plastic strain value will increase with the fatigue crack propagation. In combination

with the fatigue crack propagation path at the U-rib welding toe with residual stress considered in Fig. 13, it can be found that the plastic deformation is mainly at the crack surface and crack tip area, and the equivalent plastic strain in other areas at the U-rib-diaphragm joint is zero. Through measurement, the plastic zone sizes of 30,000 load cycles, 200,000 load cycles and 250,000 load cycles were 2.26mm, 3.4mm and 4.46mm, respectively, the corresponding surface crack lengths were 17.36mm, 27.83mm and 29.43mm, and the ratio of the plastic zone to the crack length was small. Larger plastic zone appeared in the diaphragm plate on the left side of the crack tip of the crack tip cell by inhibiting crack after loading cycle 30,000 times, diaphragm plate on the right side of the crack tip during the load cycle extended continuously, the crack tip plastic zone is small is always less than 1 mm, so the linear elastic fracture mechanics can be thought of and the interaction integral method based on the theory of the *J* integral of the residual stress field in the U-rib toe fatigue crack propagation analysis still apply.

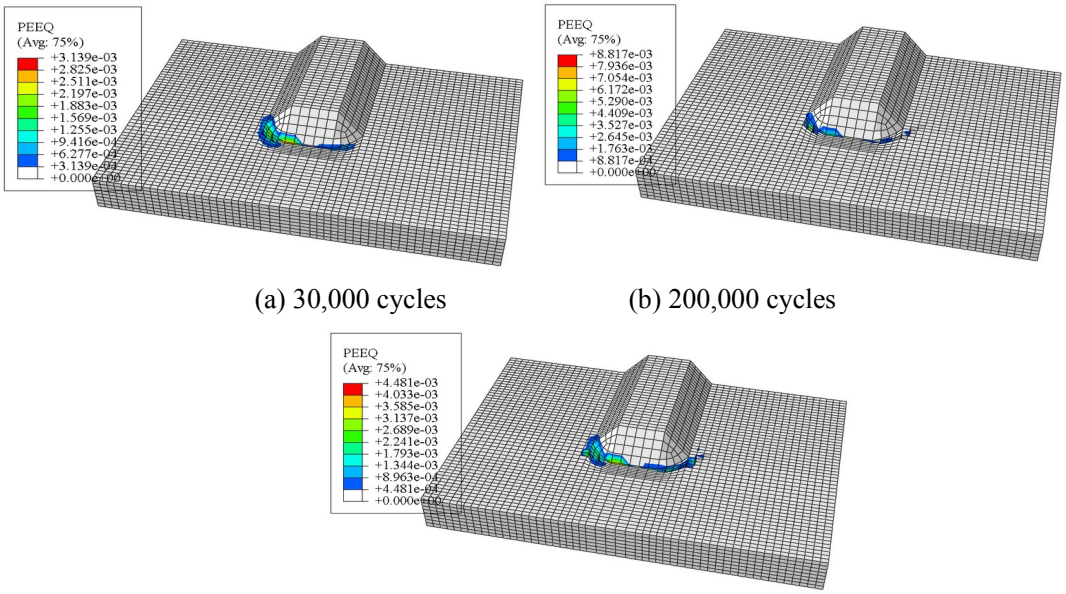

(a) 30,000 cycles (b) 200,000 cycles

(c) 250,000 cycles

Fig. 16 The equivalent plastic strain in the crack tip area of U-rib welding toe when the residual stress field is introduced

Considering the influence of the plastic zone, the residual stress intensity factor corresponding to the residual stress site was calculated by using the interaction integral to obtain the sum of the stress intensity factor K_{I}, namely the cumulative stress intensity factor, of the type I crack in the U-rib welding toe during the loading cycle when the residual stress field was considered, as shown in Fig. 17. It can be seen that the cumulative residual stress intensity factor is always positive and shows an increasing trend, indicating that when considering the residual stress field, the residual tensile stress generated by the welding residual stress field is greater than the residual compressive stress generated by plastic deformation for the fatigue crack at the U-rib welding toe, and crack closure will not occur during the fatigue crack propagation process. By comparing the cumulative residual stress intensity factor and the value of the stress intensity factor generated by the cyclic load, it can be seen that the ratio between the residual stress intensity factor and the cyclic load is larger, that is, when the equivalent stress ratio is larger than *R*, the fatigue crack propagation at the U-rib toe will be accelerated. The equivalent stress ratio is defined in formula (16).

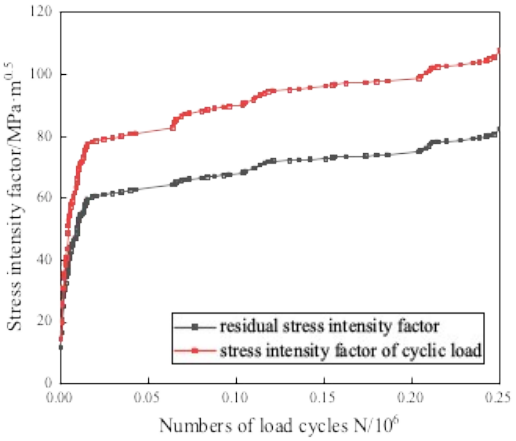

Fig. 17 Cumulative stress intensity factor of fatigue crack in U-rib toe when residual stress field is introduced

4.3 Analysis of fatigue crack propagation rate

The relationship between the length of the crack 2*c* along the long axis of the initial crack and the number of load cycles *N* of the fatigue crack at the U-rib toe was analyzed. Fig. 18 shows the 2*c*-*N* curve without considering the residual stress field. It can be seen that under the single action of the vehicle load, before the load cycle of 200,000 times, no plastic deformation occurs at the fatigue crack tip, and the two curves coincide, that is, the crack propagation rate is the same under both plastic and non-plastic conditions. The crack propagation rate is the same under both plastic and non-plastic conditions. Considering the plastic fatigue crack of the material, the length of the crack reached 25mm when the load cycle was about 1.5 million times, while the length of the fatigue crack without plastic consideration reached 25mm when the load cycle was about 3 million times, indicating that the fatigue crack propagation rate at the U-rib toe with plastic consideration was slightly higher than that without plastic consideration. The reason may be that the plastic deformation of crack tip increases the increment of energy release rate.

Similarly, Fig. 19 shows the relationship between the length of the crack 2c along the long axis of the initial crack and the number of load cycles N of the fatigue crack at the U-rib toe when the residual stress field is considered. As the stress intensity factor generated by the residual stress field of welding is large and always positive, the equivalent stress ratio *R* is increased, and the corresponding equivalent stress intensity factor amplitude increases, finally leading to the increase of crack propagation rate. It can be intuitively seen from Fig. 20 that before 20,000 load cycles, when considering plasticity and equivalent stress ratio *R*, the curve slope of fatigue crack length and cycle times at U-rib welding toe is the largest, indicating that the propagation rate is the fastest at this time. Before a 150000 - cycle, considering material plastic deformation U-rib weld toe of the fatigue crack propagation rate is significantly higher than without considering the plastic extension rate, after considering plastic deformation U-rib fatigue crack is mainly extend along U-rib thickness direction, without considering the plastic deformation and fatigue crack along the long axis direction of 2c extensions, lead to the late without considering plastic deformation of crack propagation is faster. However, from the analysis of the whole cycle process, the U-rib fatigue crack with plastic deformation considered after 250,000 cycles, the crack length along the long axis direction is 30mm, the crack depth along the short axis direction is 6mm, and after 250,000 cycles, the length of the U-rib fatigue crack along the long axis direction is about 25mm, the crack depth along the short axis direction is 5.88mm, which show that the fatigue crack propagation rate is higher in the whole cycle considering plastic

deformation and equivalent stress ratio *R*.

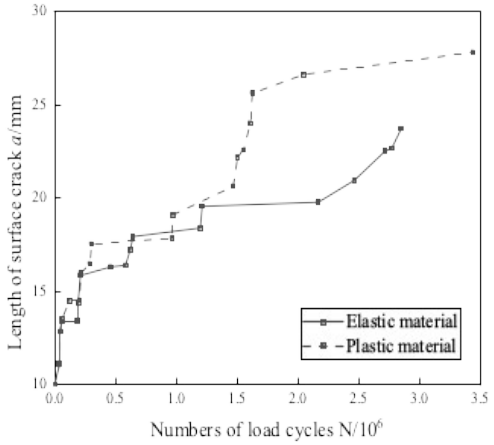

Fig. 18 Fatigue crack propagation rate of U-rib weld toe without residual stress field

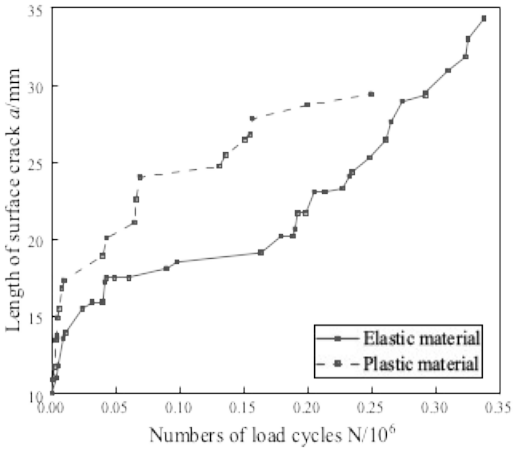

Fig. 19 Fatigue crack propagation rate of U-rib weld toe with residual stress field

5 Conclusion

In this paper, by introducing *Chaboche* elastoplastic constitutive relation, using the XFEM analysis of the orthotropic bridge deck U-rib weld toe of the fatigue crack propagation law, based on the interaction integral method to obtain the crack propagation process, each cycle load down load to zero component internal residual stress and the crack tip stress intensity factor, and analyzed the influence of welding residual stress on the law of crack propagation. The following conclusions are drawn:

(1) For the fatigue crack propagation path, when considering the plastic deformation of the member, the fatigue crack at the U-rib toe basically remains unchanged in the short-axis direction of the initial crack, but increases along the long-axis direction. Compared with linear elastic materials, the crack propagation trend is more consistent with the actual crack propagation trend in Bridges. In the process of crack propagation, because the plastic zone of the crack tip on one side of the diaphragm is larger than that on the other side, the crack propagation on that side will be inhibited, and the inhibition effect will be more significant when the residual stress field is considered. The reason may be that residual compressive stress is generated at the crack tip of one side of the larger plastic zone, resulting in the stress intensity factor here lower than that of the other side of the crack, and thus inhibited propagation.

(2) by analyzing the load down load to zero each time the loop of the crack tip stress intensity factor, can be found, when not to consider when the welding residual stress field, U-rib weld toe of the fatigue crack tip plastic zone is small, plastic deformation, the stress intensity factor of the residual compressive stress, the stress intensity factor of crack opening is very small, less than 1 $MPa\cdot m^{0.5}$, shows no welding residual stress field, the crack closure effect due to plastic deformation for U-rib weld toe of the influence of the fatigue crack propagation can be ignored. When considering the residual stress field of welding, the crack tip region is in the state of residual tensile stress each time the crack propagates, and the crack closure will not occur during the fatigue crack propagation process.

(3) Analyze the relationship between the crack length $2c$ in the long axis direction of the initial crack and the

number of load cycles *N* of the fatigue crack of U-rib toe. The results show that when the residual stress field is not considered, the fatigue crack propagation rate at U-rib toe with plasticity considered is significantly higher than that without plasticity because the plastic deformation of the member will affect the energy release rate amplitude. When the residual stress field is introduced, due to the joint influence of plastic deformation and equivalent stress ratio *R*, the increment of equivalent energy release rate during the fatigue crack propagation process is increased, and the fatigue crack propagation rate at U-rib toe is correspondingly increased.

Declaration of conflicting interests

The authors declared no potential conflicts of interest with respect to the research, authorship, and/or publication of this article.

Funding support

The works described in this paper are substantially supported by the grant from the National Natural Science Foundation of China (Grant No. 51678135); the Natural Science Foundation of Jiangsu Province (No. BK20171350); Six Talent Peak Projects in Jiangsu Province (JNHB-007), which are gratefully acknowledged.

References

[1] Ji Bohai, XU Jie, YAO Yue, et al. Fatigue damage analysis of rib-to-deck weld joints of steel bridge deck considering load influence surface [J]. Journal of Chongqing Jiaotong University(Natural Science), 2019, 38(11): 27-33.

[2] QU Yu, ZENG Yong, GU Anbang, et al. XFEM and its application in fatigue crack propagation of orthotropic steel bridge deck[J]. Journal of Chongqing Jiaotong University (Natural Science), 2018, 37(4): 21-27.

[3] Kim J H, Lee S B. Prediction of crack opening stress for part- through cracks and its verification using a modified strip-yield model[J]. Engineering Fracture Mechanics, 2000, 66: 1- 14.

[4] Zhang Bin, Guo Wanlin. Numerical simulation of surface crack propagation considering the crack closure effects and the three-dimensional stress constraints[J]. Chinese Journal of Computational Mechanics, 2005, 22(6):

[5] Qu Xianqiang, Shi Dexin, Cui Hongbin, et al. Crack closure model in residual stress field of welding[J]. Journal of Harbin Engineering University, 2006(5): 686- 689.

[6] Liu Zhongxiang. Research in Numerical Simulation of Fatigue Crack Propagation in Long-span Steel Bridges[D]. Nanjing: Southeast University, 2015

[7] Wei Xing, Jiang Su. Fatigue Life Prediction on Rib-to-Deck Welded Joints of Steel Bridge Deck Based on LEFM[J]. Journal of Southwest Jiaotong University, 2017, 52(1): 16-22.

[8] Wang Benjin, De Backer H, Chen Airong. A Homogenization Method on Crack Growth on Orthotropic Steel Decks[J]. China J. Highw. Trasp., 2017, 30(3): 113-158.

[9] Qu Yu. Study on Fatigue Mechanism of Orthotropic Deck of Steel Bridge with Box Girder[D]. Chongqing: Chongqing Jiaotong University, 2018

[10] Wang Chunsheng, Zhai Musai, Tang Youming, et al. Numerical Fracture Mechanical Simulation of Fatigue Crack Coupled Propagation Mechanism for Steel Bridge Deck[J]. China J. Highw. Transp., 2017, 30(3): 82-95.

[11] X H Zhou, K Huang. Research on Fatigue Cracking Characteristics and Reinforcement Method for Butt Welded Joints of U-Ribs in Steel Bridge Deck [J]. Journal of China & Foreign Highway, 2019, 29(3): 138-142

[12] Qu Yu, Gu Anbang, Zeng Yong, et al. Study on The Crack Plastic Zone of Bridge Structure Steel and Its Application[J]. Journal of Southwest Jiantong University, 2018, 53(4): 720-726

[13] Shih C F, Asaro R J. Elastic-plastic analysis of cracks on biomaterial interface: part I-small scale yielding[J]. Journal of Applied Mechanics, 1988, 55(2):299-316.

[14] Ma Zicong. Study on Residual Fatigue Life Prediction for Crack Damaged Offshore Platform Structures[D].Dalian: Dalian University of Technology, 2018

[15] Walker K. The effect of stress ratio during crack propagation and fatigue for 2024-T3 and 7075-T6 aluminum[M]//Effects of environment and complex load history on fatigue life. ASTM International, 1970.

[16] Japan Society of Steel Construction(JSSC). Fatigue design recommendations for steel structures and commentary[S].

[17] Chuang Cui, Qinghua Zhang, Yi Bao, et al. Fatigue life evaluation of welded joints in steel bridge considering residual stress[J]. Journal of Constructional Steel Research. 2019, 153: 509-518.

[18] Elber W. The significance of fatigue crack closure[J]. Damage Tolerance in Aircraft Structure, 1971, ASTM STP 486: 230-242.

[19] Solanki K, Daniewicz SR, Newman Jr JC. Finite element modelling of plasticity-induced crack closure with emphasis on geometry and mesh refinement effects[J]. Engineering Fracture Mechanics, 2003, 70: 1475–89.

[20] Wu J, Ellyin F. A study of fatigue crack closure by elastic-plastic finite element analysis for constant-amplitude loading[J]. International Journal Fracture, 1996, 82: 43–65.

[21] P.F.P. de Matos, D Nowell. On the accurate assessment of crack opening and closing stresses in plasticity-induced fatigue crack closure problems[J]. Engineering Fracture Mechanics, 2007, 74: 1579-1601.

[22] Zhao Lili. Numerical Simulation of The Effect of Shot Peening Residual Stress on Crack Growth Fatigue Life[D]. Jinan: Shandong University, 2015

[23] Wang Meng, Qian Fengxia, Yang Weiguo, et al. Comparison Study on Constitutive Relationship of Low Yield Point Steels, Q345B Steel and Q460D Steel [J]. Engineering Mechanics, 2017, 34(2): 60-68.

[24] Zhao Qiu, Wu Chong. Numerical Analysis of Welding Residual Stress of U-rib Stiffened Plate [J]. Engineering Mechanics, 2012, 29(8): 262-268.

[25] Kang Ling. Numerical Simulation of Welding Residual Stress in Both Longitudinal and Transverse Ribs of Orthotropic Steel Deck [D]. Chengdu: Southeast Jiaotong University, 2015

[26] Sun Zhenghua. Multi-Scale Modeling dealing with Local Details for Long Span Steel Bridges and its Applications[D]. Nanjing: Southeast University, 2006

[27] JTG D64-2015. Code for design of steel structures of Highway Bridges[S]. Beijing: People's Communications Press, 2015